Lateral change of in-plate stress and outer-rise seismicity along the southern Mariana trench

Jiangyang Zhang[1], Hongfeng Yang[2], Han Chen[2], Fan Zhang[3], Gaohua Zhu[2], and Zhen Sun[4]

[1]South China Sea Institute Of Oceanology
[2]The Chinese University of Hong Kong
[3]South China Sea Institute of Oceanology, Chinese Academy of Sciences
[4]CAS Key Laboratory of Ocean and Marginal Sea Geology, South China Sea Institute of Oceanology

November 23, 2022

Abstract

We modeled the bending deformation of the subducting plate at the southern Mariana using a 3-D elastic plate flexural model. Intraplate stresses were investigated, with the along-strike variable boundary loadings. In order to match the observed plate geometry, boundary vertical loading near the Challenger Deep had to be set twice of that in the region further east within our study area. By comparing results between 2-D and 3-D models, we found that the difference on estimating plate stress can exceed 20% when there is an along-strike variation in plate bending. Finally, we found that the sharp lateral variation in the σ and the σ corresponded to an outer-rise earthquake cluster at the southern Mariana subduction zone, indicating that along-strike variation in σ and σ may be a significant mechanism to cause non-uniform distribution of outer-rise earthquakes.

Hosted file

`supporting information_grl.docx` available at https://authorea.com/users/541854/articles/601469-lateral-change-of-in-plate-stress-and-outer-rise-seismicity-along-the-southern-mariana-trench

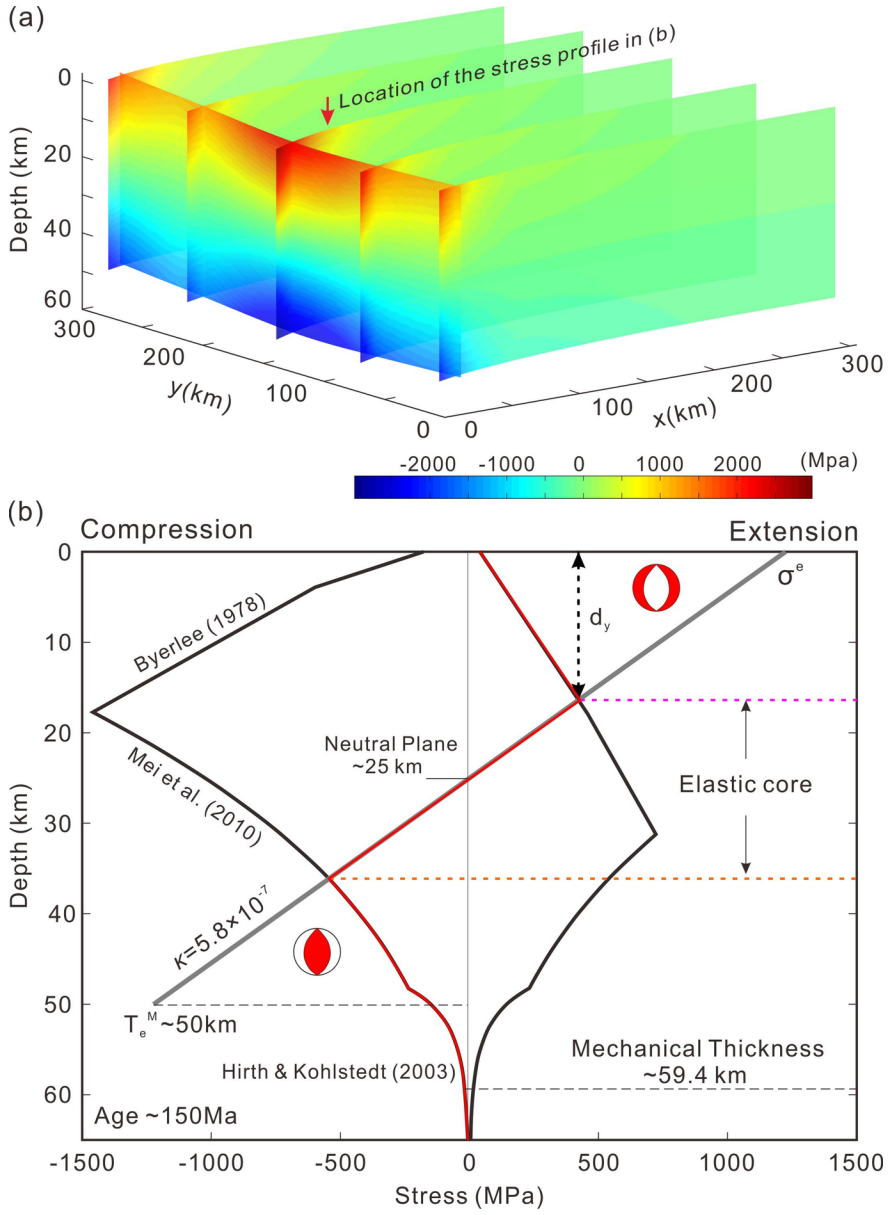

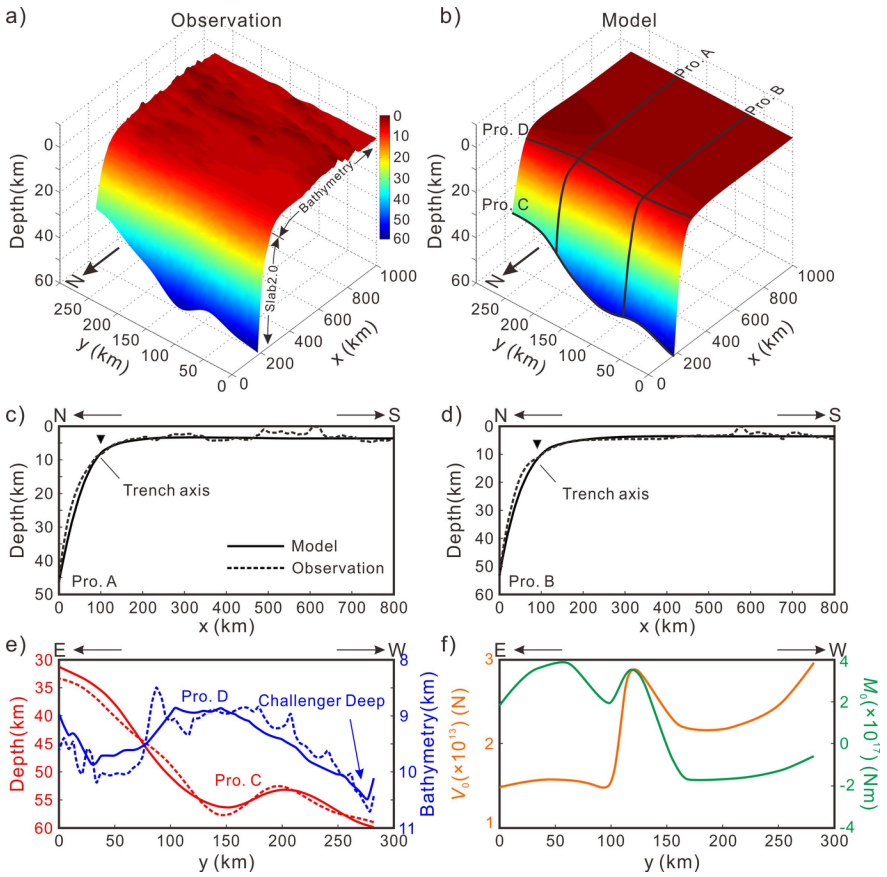

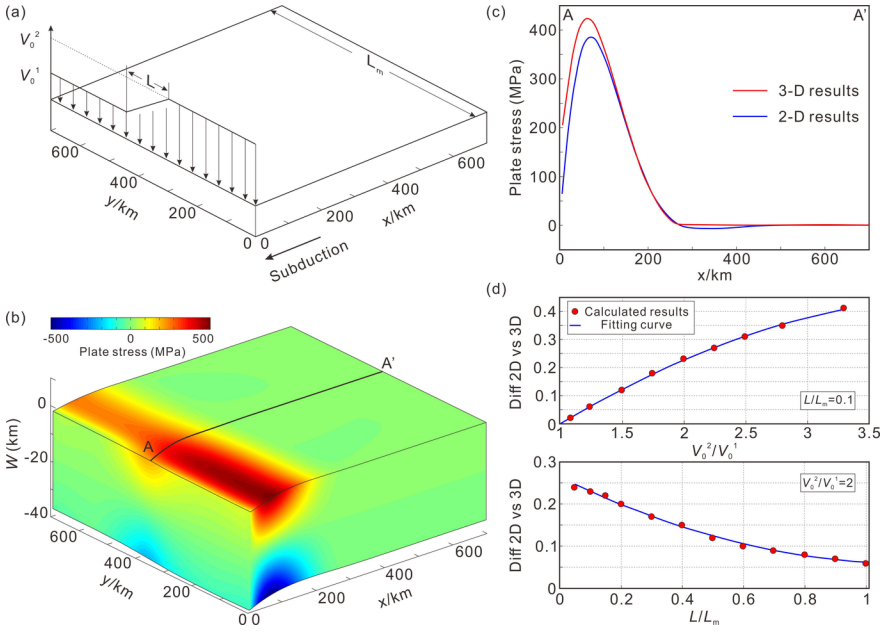

Lateral change of in-plate stress and outer-rise seismicity along the southern Mariana trench

Jiangyang Zhang[1, 2], Hongfeng Yang[2, 1]*, Han Chen[2], Fan Zhang[3], Gaohua Zhu[2], and Zhen Sun[3]

[1]. *Shenzhen Research Institute, The Chinese University of Hong Kong, Shenzhen, 518057, China*

[2]. *Earth System Science Programme, The Chinese University of Hong Kong, Shatin, NT, Hong Kong, China.*

[3]. *CAS Key Laboratory of Ocean and Marginal Sea Geology, Chinese Academy of Sciences, South China Sea Institute of Oceanology, Guangzhou 510301, China.*

* Corresponding author, Hongfeng Yang (hyang@cuhk.edu.hk)

Abstract

We modeled the bending deformation of the subducting plate at the southern Mariana using a 3-D elastic plate flexural model. Intraplate stresses were investigated, with the along-strike variable boundary loadings. In order to match the observed plate geometry, boundary vertical loading near the Challenger Deep had to be set twice of that in the region further east within our study area. By comparing results between 2-D and 3-D models, we found that the difference on estimating plate stress can exceed 20% when there is an along-strike variation in plate bending. Finally, we found that the sharp lateral variation in the σ^{e}_{yy} and the σ^{e}_{xy} corresponded to an outer-rise earthquake cluster

at the southern Mariana subduction zone, indicating that along-strike variation in σ^{e}_{yy} and σ^{e}_{xy} may be a significant mechanism to cause non-uniform distribution of outer-rise earthquakes.

Plain Language Summary

Two tectonic plates converge at subduction zones. When a plate is subducted beneath the other one, it bends and thus in-plate stress increases. If the bending stress exceeds the yield strength of the lithosphere, it produces normal faults and earthquakes at the outer rise. In our study, we simulate the bending deformation of the subducted plate at the southern Mariana subduction zone and calculate corresponding stresses using a 3-D plate bending model. We find a significant difference between 2-D and 3-D models on estimating plate bending stress when there is an along-strike change in how much the plate bends. The along-strike variation in plate bending stress may control the distribution of outer-rise earthquakes.

Key words: Mariana Subduction zone; Plate bending; Numerical simulation; Stress; Earthquakes

1. Introduction

Widely distributed subduction zone earthquakes may trigger large tsunami and cause significant loss of life and damage (e.g. Gusman et al., 2009; Lay et al., 2010). In addition to interplate earthquakes, intra-plate earthquakes can also be devastating, as seen by the 1977 Sumba Indonesia (Sunda trench, M_w=8.3) (Lynnes & Lay, 1988), the 1990 Mariana Trench (M_w=7.3) (Yoshida et al., 1992), the 2007 Kuril Trench (M_w=8.1)

(Ammon et al., 2008), and the 2009 Somoa-Tonga (M_w=8.1, Beavan et al., 2010; Lay et al., 2010) earthquakes. All of these earthquakes occurred in the outer rise region seaward of the trench, where normal faults are generated or reactivated by plate bending (Mortera-Gutiérrez et al., 2003; Ranero et al., 2003; 2005). Outer rise earthquakes may be temporally linked to large, megathrust earthquakes (Ammon et al., 2008; Beavan et al., 2010; Lay et al., 2010). Therefore, evaluating plate bending, stress distribution, and corresponding earthquakes in the outer rise region are crucial to assess earthquake and tsunami hazard in subduction zones.

Previous studies have recognized the important role of intraplate stress within the subducting plate in outer rise earthquakes (Chapple & Forsyth, 1979; Scholz & Campos, 1995; Emry et al., 2014; Zhou et al., 2015, 2018) and relationship between intraplate and interplate stress (Christensen and Ruff, 1983, 1988). For instance, Chapple and Forsyth (1979) explained the depths of tensional and compressional outer rise earthquakes using the idea that plate bending can produce tensional and compressional stress regime, separated by a neutral plane. This model was supported by focal mechanism solutions of outer rise earthquakes, e.g. along the Mariana subduction zone where the focal depths of normal and thrust faulting events delineate the boundary between the extension and compression stress regimes (Emry et al., 2014). Zhang et al., (2014) simulated the geometry of the subducted plate along the profile perpendicular to the Mariana Trench using a two-segment effective elastic thickness (T_e) flexural model. They suggested that the plate bending stresses could exceed the lithosphere yield strength envelope (YSE) and thus result in faulting and tensional earthquakes in the upper plate, corresponding to

64 the reduction in T_e. Their results showed a 21-61% reduction in T_e along the Mariana
65 subduction zone.

66 All of their work are based on 2-D flexural models, which only consider the bending
67 or slab pull from the direction perpendicular to the trench and imply that the flexural
68 parameters (including bending moment ($-M_0$), vertical shear loading ($-V_0$) and in-plate
69 stress) do not change along the strike of the trench. However, recent works clearly show
70 along-strike variation in faulting types and depths of outer rise seismicity, e.g. the northern
71 and southern Mariana subduction zone (Emry et al., 2014) where pervasive normal faults
72 are observed (Figure 1). Moreover, observations of strike-slip earthquakes in outer rise
73 further indicate complex stress fields and thus require investigations considering laterally
74 varying boundary conditions and loadings (Emry et al., 2014), rather than 2-D plate
75 bending models.

76 Some 3-D plate bending models have been developed to investigate the subducted
77 plate geometry (Manríquez et al., 2014) and boundary loading variation (Zhang et al.,
78 2018). However, no models have provided constraints on in-plate stress. Here we develop
79 a 3D model by incorporating bathymetries of the incoming plate, geometries of the
80 subducting slab, and M_0 and V_0. We then apply this model in the southern Mariana
81 subduction zone and derive stress distribution within the incoming plate, for the first time.
82 The distribution of surface elastic stress is compared to the earthquake locations that
83 were obtained from the recently acquired seismic data (Zhu et al., 2019). In the end we
84 discuss the possible relationship between the plate bending, stress, and the distribution of
85 outer rise normal fault earthquakes.

2. Data and method

2.1. Data Preparation

Three kinds of data were used in our study, including 15 arc-second resolution global bathymetry data (Tozer et al., 2019) and local multibeam data with ~150m resolution (data from the NOAA website: https://www.ngdc.noaa.gov/maps/autogrid/), global slabs geometry data (Slab 2.0 from Hayes, 2018), and newly acquired ocean bottom seismic data (Zhu et al., 2019). Firstly, we identified the strike of the bending-related normal faults from the multibeam data, as did in Ranero et al. (2005) for the Mid-America and the Chile Trench. Rose diagrams of the fault strikes help us to determine the bending direction of the plate (Figure1b and d). In order to make the plate boundary parallel to the strike of the normal fault, the model area was chosen following the bending direction (red rectangle in the Figure 1a). Then, the bathymetry data and Slab2.0 data are stitched together to provide better constraints on 3-D plate bending models.

2.2. Flexure model and inversion

We often approximate the plate as elastic layer on an inviscid layer and the flexure deformation of the elastic layer can therefore be modeled by an elastic thin plate under applied external forces (Watts, 2001; Turcotte & Schubert, 2014). At subduction zones, if the plate bending exceeds the lithospheric yield strength, it can result in bending-related normal faults, leading to earthquakes and mantle serpentinization near the outer rise

106 (Grevemeyeretal.2005; Ranero et al. 2005). This process may result in the loss of
107 strength and flexural rigidity of the lithosphere (Contreras-Reyes & Osses, 2010).
108 Therefore, a plate bending model with variable flexural rigidity was usually used to model
109 the deformation of the subducted plate (Zhang et al., 2014; Hunter & Watts, 2016; Zhang
110 et al., 2018).

111 The flexure model and inversion method used in this paper are similar to Zhang et
112 al., (2018) (See details in Supporting Information). The plate deflection *w* was inverted by
113 solving the 3-D plate flexure equation with the finite difference method (FDM), as well as
114 the Particle Swarm Optimization (PSO) inversion method. The details of methodology
115 have been described in Zhang et al., (2019). For simplicity, the T_e was divided into two
116 parts (T_e^M and T_e^m) in our model similar to previous studies (Contreras-Reyes & Osses,
117 2010; Zhang et al., 2014). The T_e^M represents the seaward T_e where the curvature of plate
118 is zero (Contreras-Reyes & Osses, 2010) and the T_e^m stands for landward T_e deduced by
119 normal faults and serpentinization. The relationship between T_e and oceanic plate age is
120 controversial. Some studies suggest there was no correlation (Bry & White 2007; Craig &
121 Copley 2014), or a weak correlation between the two (Contreras-Reyes & Osses 2010);
122 while other research indicate a strong relationship (Hunter & Watts, 2016; Zhang et al.,
123 2018). However, the T_e^M at the southern Mariana Trench in different studies are close
124 (~58km at Hunter & Watts (2016); 50km at Zhang et al., 2014; Zhang et al., 2018). The
125 T_e^M is therefore set to a constant (50km) in our model (Following the work of Zhang et al.,
126 2014). T_e^m can vary freely along the strike of the trench.

127 The calculated area is set to a rectangle with *x* axis perpendicular to the trench and

y axis along the trench (Figure 1d). The trench axis was set to be ~100km away from the boundary and the subducted plate geometry was constrained by Slab2.0 (references). If the curved trench was set to be the loading boundary, it may not be reflective of the bending direction of plate because the direction of trench strike is variable (Figure 1d). Thus we set the boundary as the deep slab, which has at least two advantages. One is that it keeps the outer rise area away from the boundary, so the boundary effect can be avoided. The other one is that it can help us better handle the effect caused by the local topographic reliefs (such as seamounts), because our aim is to model the first-order deformation of the subducting plate and thus the local topographic reliefs are noise to be removed in our simulation. Both bending moment (M_0) and vertical shear force (V_0) vary along the boundary. The squared *RMS* (root mean square) error W_{rms} between the observed data and the modeled flexure is used to find the best-fit model.

2.3. In-plate stress distribution

For thin elastic plates, the components of the plane stress along the *x* and *y* axis depending on the distance from the neutral plane (*z*) are given by:

$$\begin{bmatrix} \sigma_{xx} \\ \sigma_{yy} \\ \tau_{xy} \end{bmatrix} = -\frac{Ez}{1+\mu} \begin{bmatrix} \frac{1}{1-\mu} & \frac{\mu}{1-\mu} & 0 \\ \frac{\mu}{1-\mu} & \frac{1}{1-\mu} & 0 \\ 0 & 0 & 1 \end{bmatrix} \begin{bmatrix} \frac{\partial^2 w}{\partial x^2} \\ \frac{\partial^2 w}{\partial y^2} \\ \frac{\partial^2 w}{\partial x \partial y} \end{bmatrix} \quad (1)$$

where *E* and *μ* represent the Young's modulus and the Poisson's ratio which are set to 7 $\times 10^{10}$ Pa and 0.25, respectively. When we discuss the elastic core and the depth of plastic deformation constrained by the YSE, these stress components are projected onto

147 the principal stress axes by:

$$\sigma_1 = \frac{\sigma_{xx} + \sigma_{yy}}{2} + \sqrt{\left(\frac{\sigma_{xx} - \sigma_{yy}}{2}\right)^2 + \tau_{xy}^2}$$

148 $$\sigma_2 = \frac{\sigma_{xx} + \sigma_{yy}}{2} - \sqrt{\left(\frac{\sigma_{xx} - \sigma_{yy}}{2}\right)^2 + \tau_{xy}^2} \quad (2)$$

149 **3. Results**

150 3.1. Statistics of fault strike at outer rise

151 In southern Mariana, the magnetic lineation is obviously oblique to the trench and
152 the bending normal faults. So it is suggested that the faults forming in the southern
153 Mariana are relatively new, not reactivated abyssal hill faults. We have identified ~260
154 bending faults from the multibeam bathymetry data using the method similar to Ranero et
155 al., 2005 (Figure 1b and c). The rose diagram shows that the main direction of the fault
156 strike is ENE (Figure 1c) and thus the green arrow shows that the bending direction is
157 NNW. These two directions help us to determine the geographical range of our model
158 (Figure 1).

159 3.2. Plate bending

160 A series of numerical models have been performed for a large range of boundary
161 loadings and effective elastic thickness. Our best-fitting model has a W_{rms} less than 1.2,
162 yielding 3D smooth model results (Figure 2b). We compare the model results with data
163 along different profiles including two perpendicular to trench, one along the trench (Figure
164 2f), and another one along the base of slab in our model. In both trench-normal profiles,

the modeled deformation matches very well with the data (Figure 2c and d). Along the base of the subducting slab, our model prediction also fits the data consistently well (Figure 2e).

Compared with these three profiles, the fit between model and data along the trench gets slightly worse. Although the overall trench matches reasonably well, we underestimate the trench depth at certain places, including the Challenger Deep (Figure 2f).

To match the plate deformation, along-strike variable loadings (M_0 and V_0) were applied on the plate boundary. The V_0 applied on the western part (near the Challenger Deep) is nearly twice as much as that of the eastern part and the M_0 changes from positive to negative in a narrow range (~100 - ~170 km) (Figure 2f).

3.3. Stresses and earthquakes distribution

According to equations (1) and (2), the distribution of surface elastic stress (Figure. S1) components σ^e_{xx}, σ^e_{yy}, σ^e_{xy} and the maximum principal stress σ^e_1 are calculated in the best-fitting model (Figure 3). The σ^e_{xx} stands for the normal stress along the *x* axis (the direction perpendicular to the trench) caused by plate bending perpendicular to the trench and it reaches maximum close to the trench axis. The σ^e_{yy} represents the normal stress along trench mainly caused by lateral flexural deformation of the plate. If the flexure morphology of the plate is invariant along the trench strike, the σ^e_{yy} will then present the same tendency with σ^e_{xx} according to the Poisson's ratio of materials. Otherwise, the σ^e_{yy} will change due to the lateral plate pull. The σ^e_{xy} represents the shear force caused by the

186 lateral plate pull, too. If no lateral plate pulling exists, the σ^{e}_{xy} is zero.

187 We find that the stress distribution associated with the plate bending is
188 heterogeneous (Figure 3). In addition, the σ^{e}_{xx} increases gradually from the outer rise to
189 the trench and reaches the maximum at the Challenger Deep (Figure 3a), consistent with
190 previous studies (Zhang et al., 2014, 2019). The σ^{e}_{yy} varies along the trench and reaches
191 the maximum at ~143° E, 11-11.5°N, corresponding to the place where M_0 and V_0 change
192 sharply (Figures 2f and 3b). The σ^{e}_{xy} changes from extension to compression (or the
193 opposite) from east to west along the trench (Figure 3c). Among the stress components,
194 the σ^{e}_{xx} is the largest, reaching the maximum of ~5 GPa. The maximum of σ^{e}_{1} exceeds 6
195 GPa (Figure 3d). We also compare the σ^{e}_{1} change and the depth of outer rise seismicity
196 along the profile A (Figures 3d and e). From west to east, there is a sudden drop of σ^{e}_{1} at
197 the distance ~40-60km (please note the stress axis is reversed), coinciding with most of
198 outer-rise earthquakes in the region. The depths of these earthquakes vary from 1to
199 ~60km with a median value of ~26km (Figure 3e).

200 **4. Discussion**

201 4.1. Comparison between the 2-D and the 3-D model on estimating the plate stress

202 The stress distribution of the flexural lithosphere could be predicted by the curvature
203 of the 2-D profile perpendicular to the trench (Hunter et al., 2016; Zhang et al., 2019). The
204 plate stress distribution can further help us constrain the lithospheric yield zone, the depth
205 of outer rise earthquakes and mantle serpentinization (Emry et al., 2014; Zhang et al.,
206 2019). Garcia et al. (2019) suggested that the amount of strain ε (as well as the stress σ)

of a flexural plate can be described by: $\varepsilon = -z\frac{\partial^2 w}{\partial x'^2}$, where x' is the horizontal coordinate axis along the direction of maximum curvature. If the flexural parameters (such as M_0 and V_0) are invariant along trench, the direction of maximum curvature is perpendicular to the trench and the plate stress estimated by the 2-D model is nearly equal to that estimated by the 3-D model. Otherwise, the direction of maximum curvature will change and point to the lowest place of the three-dimensional space. In this situation, the plate stress estimated by the 2-D profile curvature may be underestimated.

Figure 4 is an example that illustrates how along-strike variable V_0 leads to an underestimate of 2-D plate stress. Here, the V_0 is set to sectioned along-strike variation, changing from V_0^1 to V_0^2 linearly within a variation distance L (Figure 4a). As we only consider the effects of the along-strike variable V_0, the T_e is set to a constant value (35km) here. Then we compare the difference between the 2-D and the 3-D models on estimating plate stress (Figure 4c). After employing dozens of different calculation models, we find that both the change in V_0 and the variation distance L (we used L/L_m in Figure 4d, where Lm is the width of our model) can affect the model difference, in which the plate stress increases with V_0 and decreases with the variation distance L (Figure 4d). Considering the Mariana Trench, if the L/L_m equals to 0.1 and V_0^2/V_0^1 is set to 2, the difference between the 2-D and the 3-D model can exceed 20% (Figure 4).

4.2. Surface elastic stress and the Yield Strength Envelope (YSE)

The in-plate stress of the elastic plate is linearly correlated with the distance from the neutral plane of the plate (z) (Equation 1). As such, the stress varies linearly from the

maximum compressive stress to the maximum tensile stress along the traversal section of a bending plate. However, the lithosphere is not perfectly elastic and the yield strength of the lithosphere should be taken into account.

At southern Mariana, if the subducted plate is an ideal, purely elastic material, the surface elastic stress would reach ~3 GPa (Figure 5a). However, the actual plate bending stress is limited by the Yield Strength Envelope (YSE). The depth of the intersection of the YSE and elastic stress profile represents the yield zone depth (d_y) where bending-related normal earthquakes often occur (Figure 5b). Our results show that the d_y strongly depends on the σ_e (Text S3 in the Supporting Information). It means that if the σ^e is given at any place, the d_y can be estimated easily. Therefore, we can use the simulated surface elastic stress to constraint the potential first fracture zone and the distribution of outer rise earthquakes.

4.3. Lateral variation of in-plate stress and outer rise earthquakes

Along the strike of the trenches, the distribution of outer rise earthquakes is often non-uniform and the faulting types of events are also different (Okal et al., 2013; Craig et al., 2014; Emry et al., 2014). Christensen & Ruff (1988) proposed that although the lithospheric bending played a major role in inducing outer rise tensional earthquakes by placing the shallow region of outer rise in extension and causing brittle deformation, the regional compressional stress caused by the interaction between the upper and subducted plate can reduce the possibility of outer rise extensional events, such as the alternation of tensional and compressional outer rise earthquakes along the Kuril

249 subduction zone (Ammon et al., 2008).

250 Here, we proposed another possible mechanism which causes the variable
251 distribution of outer rise earthquakes - the lateral variation of in-plate stress. If there is a
252 variable boundary loading caused by deep slab pull, it will lead to the along-strike variable
253 bending depth as well as the variable plate bending stress at outer rise. We propose that
254 the bending stresses exceed the yield strength of the lithosphere due to the variable
255 loading, corresponding to the variable distribution of outer rise seismicity. Here the
256 bending stresses include not only the stress along the trench-normal direction but also the
257 stress along trench (σ^{e}_{yy} and σ^{e}_{xy}) that was caused by the laterally plate pull. Our modeled
258 stress variation coincides with earthquake distribution in the outer rise of Mariana, and
259 may likely explain other outer rise earthquake distribution in other subduction zones,
260 which can be done in future studies.

261 Previous studies have demonstrated strike-slip earthquakes at the outer rise of the
262 subduction, as seen in Sumatra (Meng et al., 2012), the Gulf of Alaska (Lay et al., 2018)
263 and the Mariana trench (Emry et al., 2014). Lay et al. (2018) suggested that the outer-rise
264 strike-slip event seems to require laterally varying plate boundary conditions rather than
265 simple 2-D plate bending. Our 3-D plate bending provides a new insight to illustrate the
266 formation of the outer-rise strike-slip earthquakes. Both seamount subduction and
267 variable slab pull may cause along-strike change of bending deformation, generating the
268 corresponding in-plate shear stress (σ^{e}_{xy}). The increase of σ^{e}_{xy} may provide a mechanism
269 to produce strike-slip earthquakes.

5. Conclusion

By analyzing the results of plate bending simulation, in-plate stress, and the distribution of outer rise earthquakes, we show that the variable boundary loadings along the strike of southern Mariana Trench caused by deep slab pull can cause not only along-strike variation in degree of plate bending, but also the along-strike variant in-plate stresses. The boundary loading applied at the Challenger Deep area is nearly twice as much as that of other areas, which can make the difference between the 2-D and the 3-D model on estimating the plate stress exceed 20%. An outer rise zone with concentrated earthquakes in the southern Mariana subduction zone corresponds to the sharp variation in the along-strike normal stress and the plane shear stress. It is therefore suggested that the 3-D effect of plate bending can be a mechanism to cause non-uniform distribution of outer rise earthquakes along trench. Besides, the σ^{e}_{xy} of subducted plate may provide a mechanism to produce strike-slip earthquakes.

6. Acknowledgements

We are grateful to Prof. Jian Lin, Dr. Xiaohuan Jiang, Xiang Chen, Suli Yao, Pengcheng Zhou and Junhao Song for useful discussion. We thank Zhongxian Zhao and Zhiyuan Zhou for offering technical assistance. GMT (Wessel and Smith 1995) was used to draw the topographic map. The bathymetry data can be found at the website: https://catalog.data.gov/dataset/srtm15-plus-estimated-topography-15-seconds-global-v1. The multibeam data with ~150m resolution can be found at the NOAA website: https://www.ngdc.noaa.gov/maps/autogrid/ and the global slabs geometry data Slab 2.0

can be found at https://www.sciencebase.gov/catalog/item/5aa1b00ee4b0b1c392e86467 (Hayes et al., 2018).

This research is supported by National Key R&D Program of China (Grant Number 2018YFC1503400), Hong Kong Research Grant Council Grants (No. 14313816，14304820), Faculty of Science at CUHK, China Postdoctoral Science Foundation (No. 2019M663119), the Guangdong NSF research team project (2017A030312002), and the National Science Foundation of China (No. 41976064).

Reference

Ammon, C.J., Kanamori, H., & Lay, T. (2008). A great earthquake doublet and seismic stress transfer cycle in the central Kuril islands. *Nature* 451, 561-566.

Beaven, J., Wang, X., Holden, C., Wilson, K., Power, W., Prasetya, G., Bevis, M., & Kautoke, R. (2010). Near-simultaneous great earthquakes at Tongan megathrust and outer rise in September 2009. *Nature* 466, 959-963

Bry, M., & White, N. (2007). Reappraising elastic thickness variation at oceanic trenches. *J. Geophys. Res.* 112. Doi: 10.1029/2005JB004190.

Byerlee, J. (1978). Friction of rocks. *Pure appl. Geophys.* 116 (4-5), 615-626.

Chapple, W.M., & Forsyth, D.W. (1979). Earthquakes and bending of plates at trenches. *J. Geophys. Res.* 84 (B12), 6729-6749.

Christensen, D.H., & Ruff, L.J. (1983). Outer-rise earthquakes and seismic coupling. *Geophys. Res. Lett.* 10, 697-700.

312 Christensen, D.H., & Ruff, L.J. (1988). Seismic Coupling and Outer Rise Earthquakes. *J.*
313 *Geophys. Res.* 93 (B11), 13,421-13,444.
314 Contreras-Reyes, E., & Osses, A. (2010). Lithospheric flexure modelling seaward of the
315 Chile trench: implications for oceanic plate weakening in the Trench Outer Rise
316 region. *Geophys. J. Int.* 182 (1), 97-112.
317 Craig, T.J., & Copley, A. (2014). An explanation for the age independence of oceanic
318 elastic thickness estimates from flexural profiles at subduction zones, and
319 implications for continental rheology. *Earth planet. Sci. Lett.* 392, 207-216.
320 Craig, T.J., Copley, A., & Jackson, J. (2014). A reassessment of outer-rise seismicity and
321 its implications for the mechanics of oceanic lithosphere. *Geophys. J. Int.* doi:
322 10.1093/gji/ggu013
323 Emry, E.L., Wiens, D.A., & Garcia-Castellanos. (2014). Faulting within the Pacific plate at
324 the Mariana Trench: Implications for plate interface coupling and subduction of
325 hydrous minerals. J. Geophys. Res. Solid Earth 119, 2076-3095.
326 Garcia, E.S., Sandwell, D.T., & Bassett, D. (2019). Outer Trench Slope Flexure and
327 Faulting at Pacific Basin Subduction Zones. *Geophys. J. Int.* DOI:
328 10.31223/osf.io/dbn8j.
329 Grevemeyer, I., Kaul, N., Diaz-Naveas, J.L., Villinger, H., Ranero, C.R., & Reichert, C.
330 (2005). Heat flow and bending-related faulting at subduction trenches: Case studies
331 offshore of Nicaragua and Central Chile. *Earth planet. Sci. Lett.* 236, 238-248.
332 Gusman, A.R., Tanioka, Y., Matsumoto, H., & Iwasaki, S-I. (2009). Analysis of the Tsunami
333 Generated by the Great 1977 Sumba Earthquake that Occurred in Indonesia. *Bull.*

Seismol. Soc. Am. 99 (4), 2169-2179.

Gvirtzman, Z., & Stern, R.J. (2004). Bathymetry of Mariana trench-arc system and formation of the Challenger Deep as a consequence of weak plate coupling. *Tectonics* 23, TC2011.

Hayes, G. (2018). Slab2 - A Comprehensive Subduction Zone Geometry Model: U.S. Geological Survey data release, https://doi.org/10.5066/F7PV6JNV.

Hirth, G., & Kohlstedt, D. (2003). Rheology of the Upper Mantle and the Mantle Wedge: A View from the Experimentalists. in *Inside the Subduction Factory*, pp. 83-105, ed. Eiler, J., *American Geophysical Union.*

Hunter, J., & Watts, A.B. (2016). Gravity anomalies, flexure and mantle rheology seaward of circum-Pacific trenches. *Geophys. J. Int.* 207 (1), 288-316.

Lay, T., Ammon, C. J., Kanamori, H., Rivera, L., Koper, K. D., & Hutko, A. R. (2010). The 2009 Samoa-Tonga great earthquake triggered doublet. *Nature* 466, 964–967.

Lay, T., Ye, L., Bai, Y., Cheung, K.F., & Kanamori, H. (2018). The 2018 M_W 7.9 Gulf of Alaska Earthquake: Multiple Fault Rupture in the Pacific Plate. *Geophys. Res. Lett.* 45, 9542–9551.

Lynnes, C., & Lay, T. (1988). Source process of the great Sumba earthquake. *J. Geophys. Res.* 93, 13,407-14,320.

Manríquez, P., Contreras-Reyes, E., & Osses, A. (2014). Lithospheric 3-D flexure modelling of the oceanic plate seaward of the trench using variable elastic thickness. *Geophys. J. Int.* 196, 681–693.

Mei, S., Suzuki, A.M., Kohlstedt, D.L., Dixon, N.A., & Durham, W.B. (2010). Experimental

356 constraints on the strength of the lithospheric mantle. *J. Geophys. Res.* 115 (B8).
357 Meng, L., Ampuero, J.P., Stock, J., Duputel, Z., Luo, Y. & Tsai, V.C. (2012). Earthquake in
358 a maze: compressional rupture branching during the 2012 M(w) 8.6 Sumatra
359 earthquake. *Science*. 337, 724–726.
360 Mortera-Gutiérrez, C.A., Scholl, D.W., & Carlson, R.L. (2003). Fault trends on the seaward
361 slope of the Aleutian Trench: Implications for a laterally changing stress field tied to a
362 westward increase in oblique convergence. *J. Geophys. Res.* 108, 2477.
363 Okal, E.A., Reymond, D., & Hongsresawat, S. (2012). Large, pre-digital earthquakes of
364 the Bonin-Mariana subduction zone, 1930–1974. *Tectonophysics.*
365 *http://dx.doi.org/10.1016/j.tecto.2012.09.006*
366 Ranero, C.R., Morgan, J.P., McIntosh, K., & Reichert, C. (2003). Bending-related faulting
367 and mantle serpentinization at the Middle America trench. *Nature* 425(6956), 367–
368 373.
369 Ranero, C.R., Villaseñor, A., Morgan, J.P., & Weinrebe, W. (2005). Relationship between
370 bending-faulting at trenches and intermediate-depth seismicity. *Geochem. Geophys.*
371 *Geosyst.* 6 (12).
372 Scholz, C. H., & Campos, J. (1995). On the mechanism of seismic decoupling and back
373 arc spreading at subduction zones, *J. Geophys. Res.*, 100 (B11), 22,103–22,115.
374 Tozer, B., Sandwell, D. T., Smith, W. H. F., Olson, C., Beale, J. R., & Wessel, P.
375 (2019). Global bathymetry and topography at 15 arc seconds: SRTM15+. *Earth and*
376 *Space Science.* Doi:10.1029/2019ea000658
377 Turcotte, D., & Schubert, G. (2014). *Geodynamics*, 3nd edn. Cambridge University Press,

pp. 626.

Watts, A.B. (2001). *Isostasy and Flexure of the Lithosphere*, 1st edn, Cambridge University Press, New York, pp. 478.

Yoshida, Y., Satake, K., & Abe, K. (1992). The large normal-faulting Mariana Earthquake of April 5, 1990 in uncoupled subduction zone. *Geophys. Res. Lett.* 19 (3), 297-300.

Zhang, F., Lin, J., & Zhan, W. (2014). Variations in oceanic plate bending along the Mariana trench. *Earth planet. Sci. Lett.* 401, 206-214.

Zhang, F., Lin, J., Zhou, Z., Yang, H., & Zhan W. (2018a). Intra- and intertrench variations in flexural bending of the Manila, Mariana and global trenches: implications on plate weakening in controlling trench dynamics. *Geophys. J. Int.* 212, 1429-1449.

Zhang, J., Sun, Z., Qiu, N., Zhang, Y., & Li, F. (2019). 3-D effective elastic thickness inversion of subduction zone based on particle swarm optimization algorithm. *Chinese J. Geophys. (in Chinese)* 62 (12), 4738-4749.

Zhang, J., Sun, Z., Xu, M., Yang, H., Zhang, Y., & Li, F. (2018). Lithospheric 3-D flexural modelling of subducted oceanic plate with variable effective elastic thickness along the Manila Trench. *Geophys. J. Int.* 215, 2071-2092.

Zhou, Z., Lin, J., Behn, M.D., & Olive, J.A. (2015). Mechanism for normal faulting in the subducting plate at the Mariana Trench. *Geophys. Res. Lett.* 42, 4309-4317.

Zhou, Z., & Lin, J. (2018). Elasto-plastic deformation and plate weakening due to normal faulting in the subducting plate along the Mariana Trench. *Tectonophysics* 734, 59-68.

Zhu, G., Yang, H., Lin, J., Zhou, Z., Xu, M., Sun, J., & Wan, K. (2019). Along-strike

variation in slab geometry at the southern Mariana subduction zone revealed by seismicity through ocean bottom seismic experiments. *Geophys. J. Int.* 218 (3), 2122-2135.

Figures

Figure 1. (a) Seafloor bathymetry of the southern Mariana Trench. The red rectangle is the domain of our 3-D flexural model; the black square box is the area where the normal faults are identified with the multi-beam data (please see Figure 1b) and the yellow star represents the location of the Challenger Deep. Yellow lines are the magnetic lineation based on Zhou et al., (2015). (b) Tectonic structure of the oceanic plate. Red lines are normal faults identified from the multibeam. (c) The rose diagram (red part) shows that the direction of strike of the bending-normal faults is ~N80˚E at the southern Marina Trench and the green arrow perpendicular to the fault strike shows that the bending direction is ~N10˚W. (d) Schematic 3-D model to illustrate the bending stresses of the subducted plate under along-strike variable loadings (bending moment (M_0) and vertical shear force (V_0) caused by deep slab pull). σ_{xx} and σ_{yy} represent the stresses on vertical profiles. σ^e_{xx}, σ^e_{yy}, and σ^e_{xy} are surface elastic stresses (The meaning of surface elastic stress is shown in Figure 5).

Figure 2. Result of our model. (a) Observed plate bending of the study area. The observation comes from the combination of the global 15 arc-second resolution

421 bathymetry data (Tozer et al., 2019) and the Slab 2.0 data (Hayes et al. 2018). (b) 3-D
422 plate bending model results. Pro. A, B, C, and D represent the profiles shown in Figure
423 2c-e. The Pro. D is along the trench axis. (c) - (e) Comparisons between our model and
424 observed data along different profiles in Figure 2(b). The dashed lines represent the
425 observation and the solid lines are results of our model. (f) The variation of inverted M_0
426 (blue line) and V_0 (orange line) along the plate boundary.
427
428 Figure 3. The components of the surface elastic stress (the meaning of the surface elastic
429 stress is shown in Figure 5). The white circles represent the location of outer rise
430 earthquakes proposed by Zhu et al., (2019) and the grey circles in are historic outer rise
431 earthquakes in this area (from USGS). Variable radiuses of circles represent the event
432 magnitudes. Focal mechanism solutions come from GCMT. (a) The distribution of σ^e_{xx}, the
433 normal stress along the direction perpendicular to the trench. The yellow star stands for
434 the location of the Challenger Deep. (b) The distribution of σ^e_{yy}, the normal stress along
435 the strike of the trench, and (c) The distribution of the plane shear stress σ^e_{yy}. (d) The
436 distribution of the maximum principal stress σ^e_1 (Please see the equation (2)). (e) The σ^e_1
437 and depth of outer rise earthquakes along the profile A-A' in Figure (d). It shows that the
438 sharp variation of the σ^e_1 along the strike of trench corresponds well to the concentrated
439 seismic zone. The histogram represents the variation of seismic depths.
440
441 Figure 4. The difference between the 2-D and the 3-D model on estimating the plate
442 stress. (a) Schematic 3-D model to illustrate the along-strike variable V_0. L is the variation

443 distance of V_0 and L_m is the width of our model. (b) The 3-D plate stress distribution under
444 the loading shown in Figure a. The difference of the surface elastic stress between the
445 2-D and the 3-D model along the profile A-A' in Figure b. (d) Plotting difference between
446 the 2-D and the 3-D model on estimating plate stress versus the change of V_0 (V_0^2/V_0^1)
447 and the L/L_m

448

449 Figure 5. The relationship between the surface elastic stress and outer rise earthquakes.
450 (a) Profiles with different direction along the southern Mariana and their bending stress
451 distributions. The red arrow is the location of the profile shown in Figure (b). (b) The YSE
452 used by Hunter and Watts (2016) which is a combination of the rheology laws of Byerlee
453 (1978), Mei et al. (2010), and Hirth and Kohlstedt (2003). The plate age at the southern
454 Mariana Trench is nearly 145-150 Ma with a mechanical thickness of ~59km. The grey
455 line represents the plate elastic stress profile and the red line represents the real stress
456 profile due to plastic deformation. The σ^e is the surface elastic stress (a theoretical value
457 in the model) and the d_y is the yield depth. It is suggested that bending-related normal
458 fault (earthquake) occurred shallower than this depth. It shows that the σ^e is positively
459 correlated with the d_y and therefore the σ^e can be used to constrain the potential first
460 fracture zone.

461

Figure01.

(a)

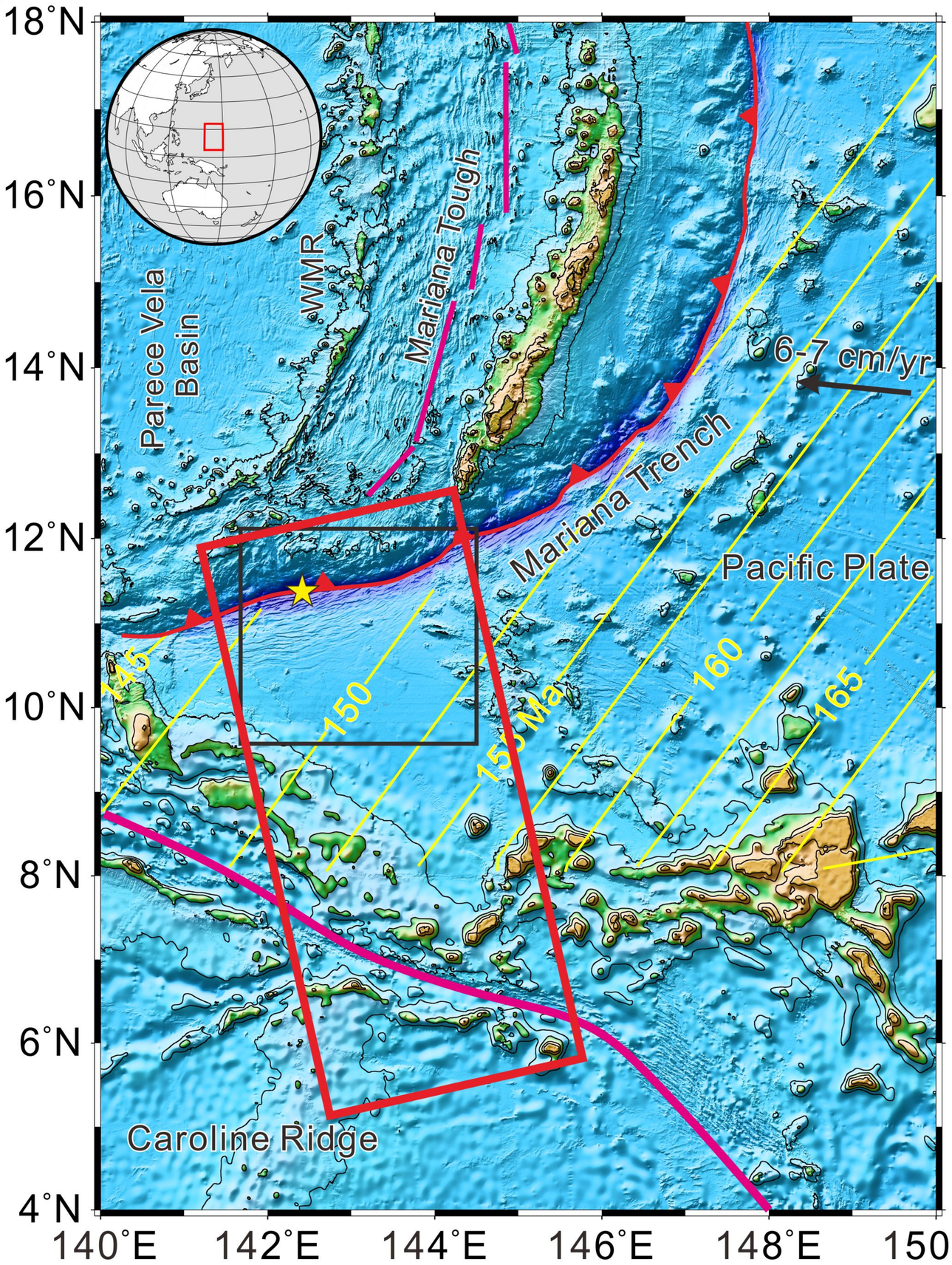
18°N
16°N
14°N
12°N
10°N
8°N
6°N
4°N
140°E
142°E
144°E
146°E
148°E
150°E
Parece Vela Basin
WMR
Mariana Tough
Mariana Trench
6-7 cm/yr
Pacific Plate
145
150
155Ma
160
165
Caroline Ridge

(b)

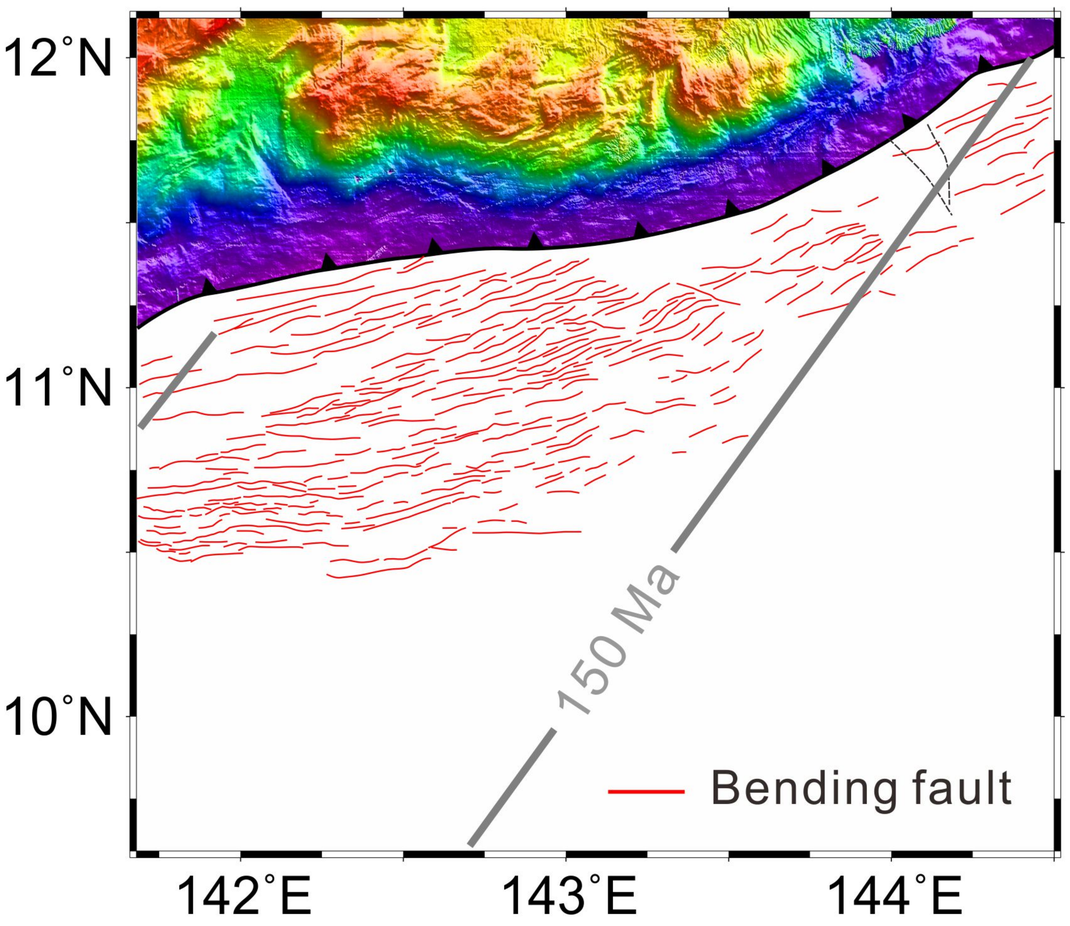
12°N
11°N
10°N
142°E
143°E
144°E
150 Ma
Bending fault

(c)

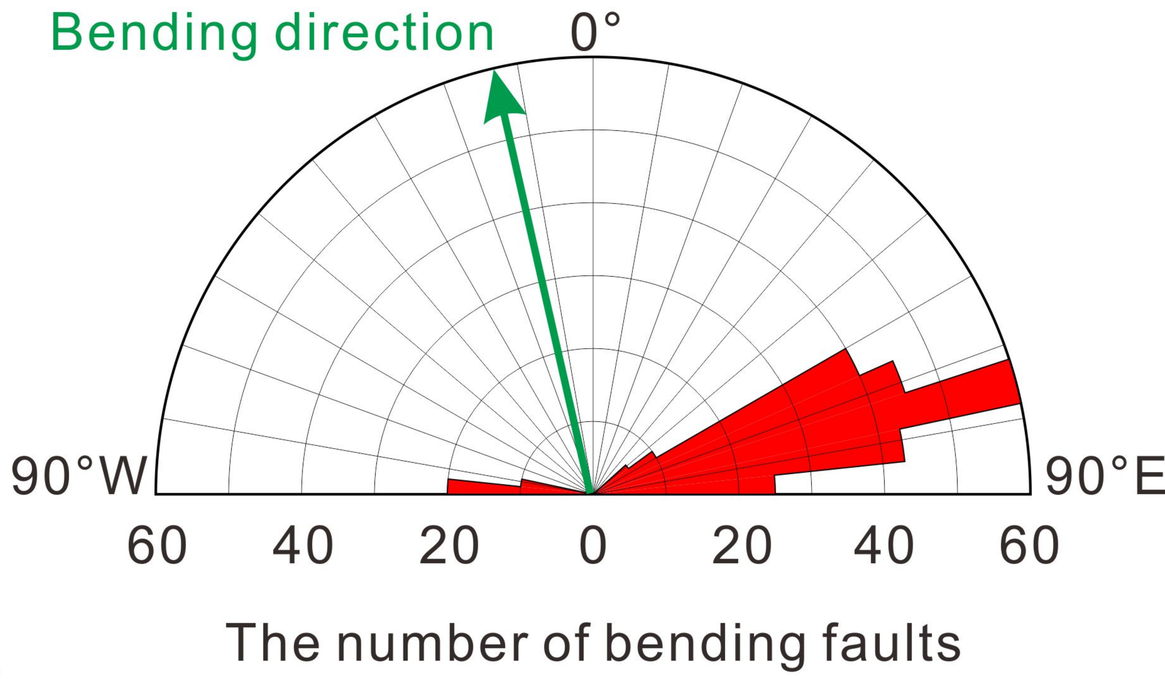
Bending direction
0°
90°W
90°E
60
40
20
0
20
40
60
The number of bending faults

(d)

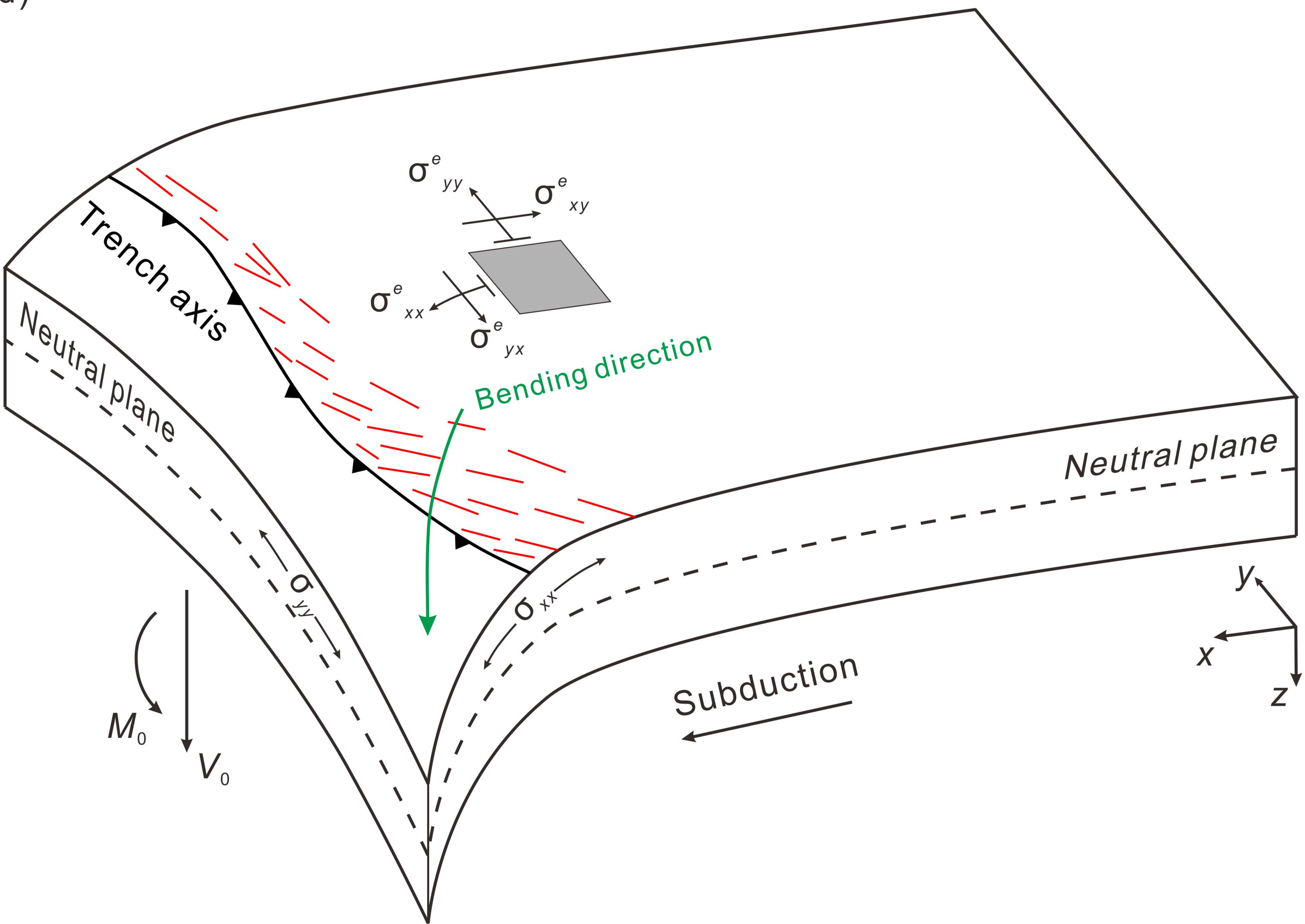
Trench axis
Neutral plane
Bending direction
Neutral plane
Subduction
σ^e_{yy}
σ^e_{xy}
σ^e_{xx}
σ^e_{yx}
σ_{xy}
σ_{xx}
M_0
V_0
y
x
z

Figure02.

a)

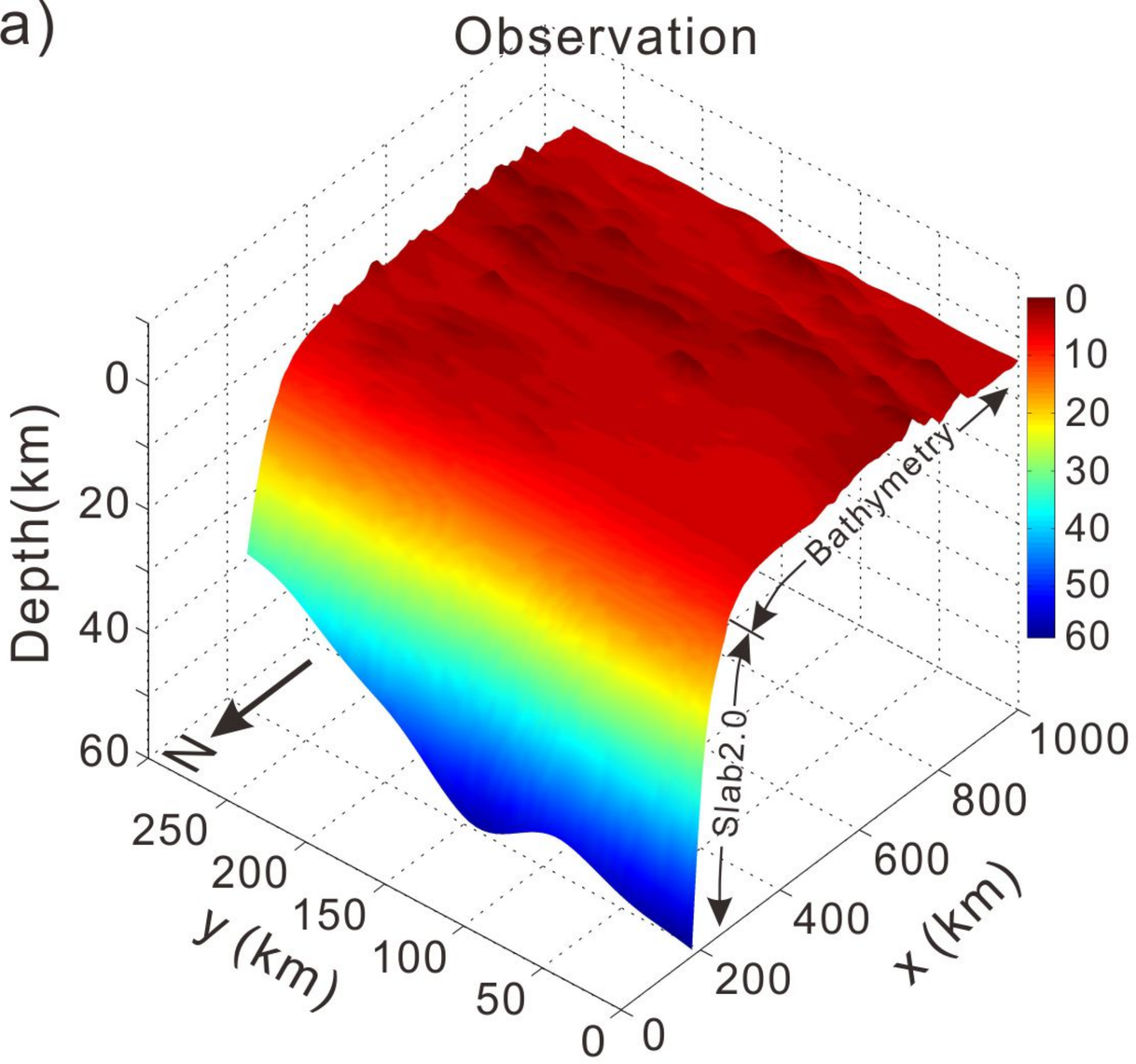
Observation
Depth(km)
0
20
40
60
N
250
200
150
100
50
0
y (km)
0
200
400
600
800
1000
x (km)
Slab2.0
Bathymetry
0
10
20
30
40
50
60

b)

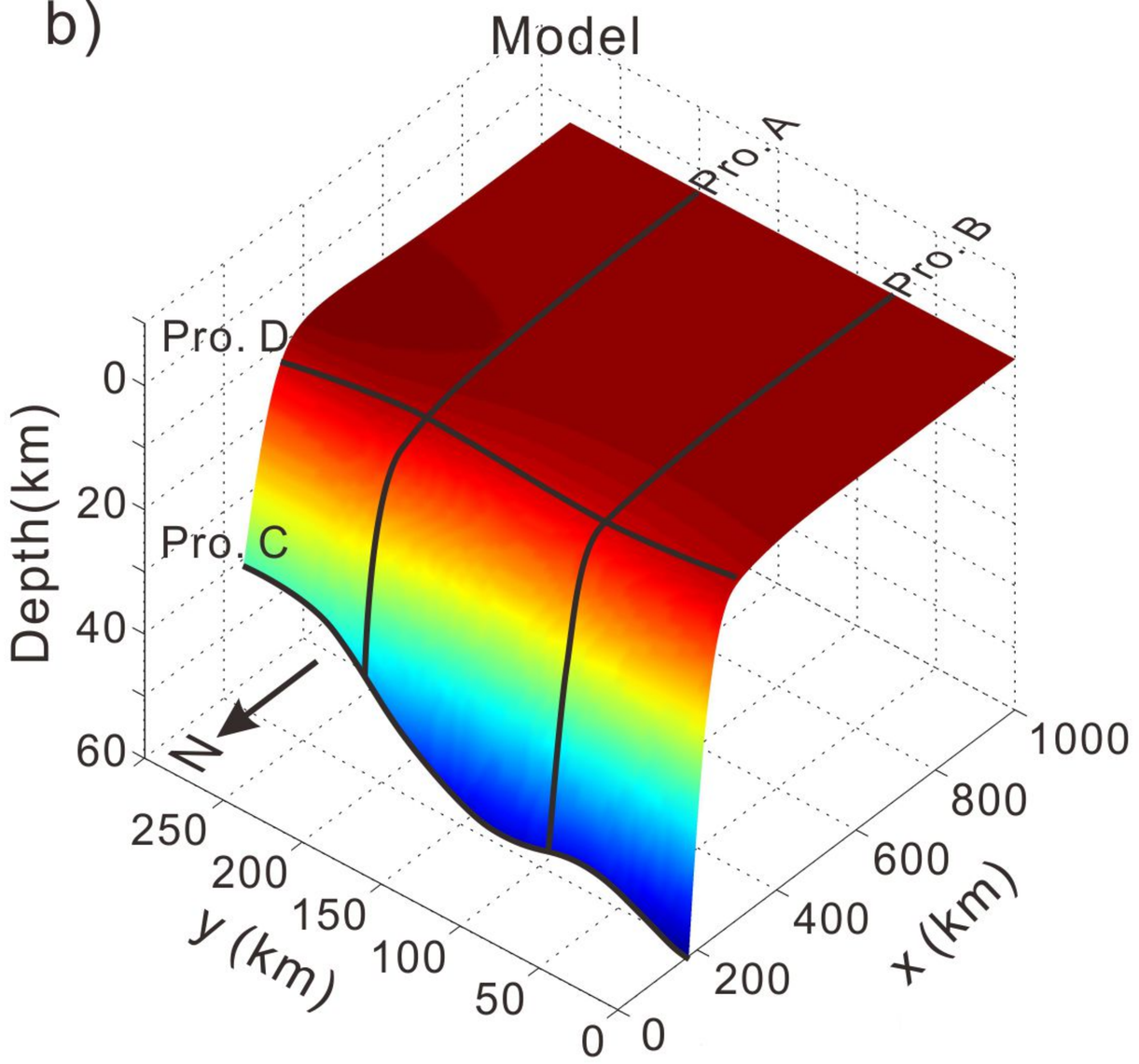
Model
Pro. A
Pro. B
Pro. D
Pro. C
Depth(km)
0
20
40
60
N
250
200
150
100
50
0
y (km)
0
200
400
600
800
1000
x (km)

c)

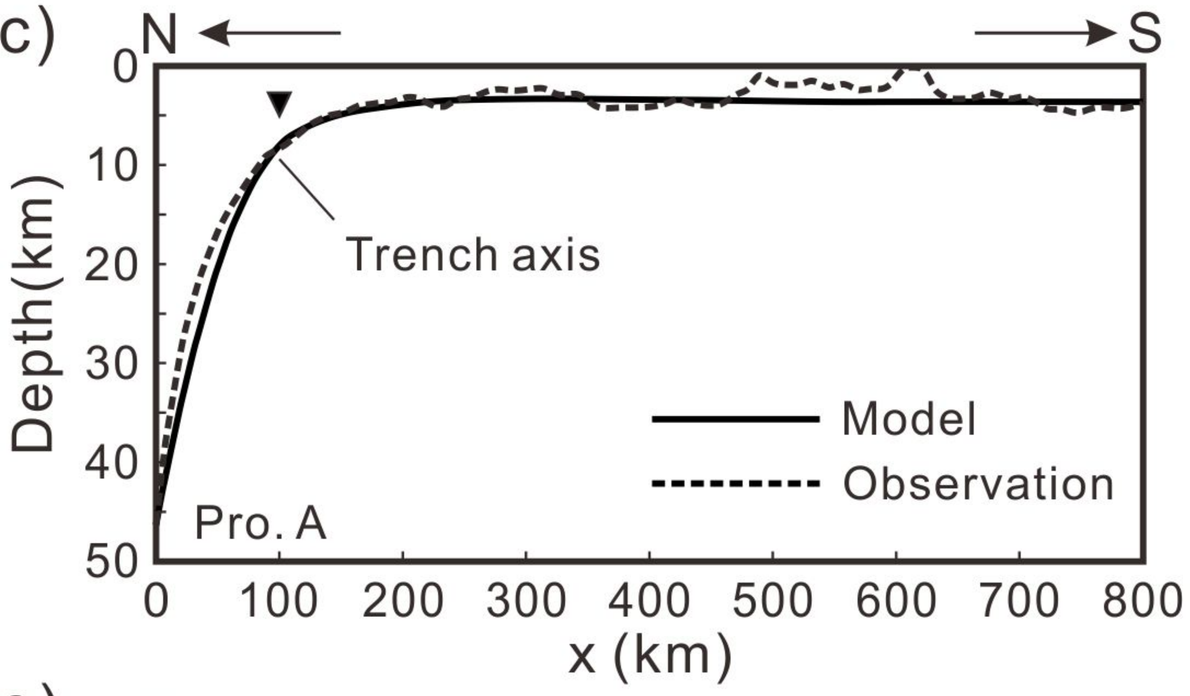
N
S
Depth(km)
0
10
20
30
40
50
Trench axis
Model
Observation
Pro. A
0
100
200
300
400
500
600
700
800
x (km)

d)

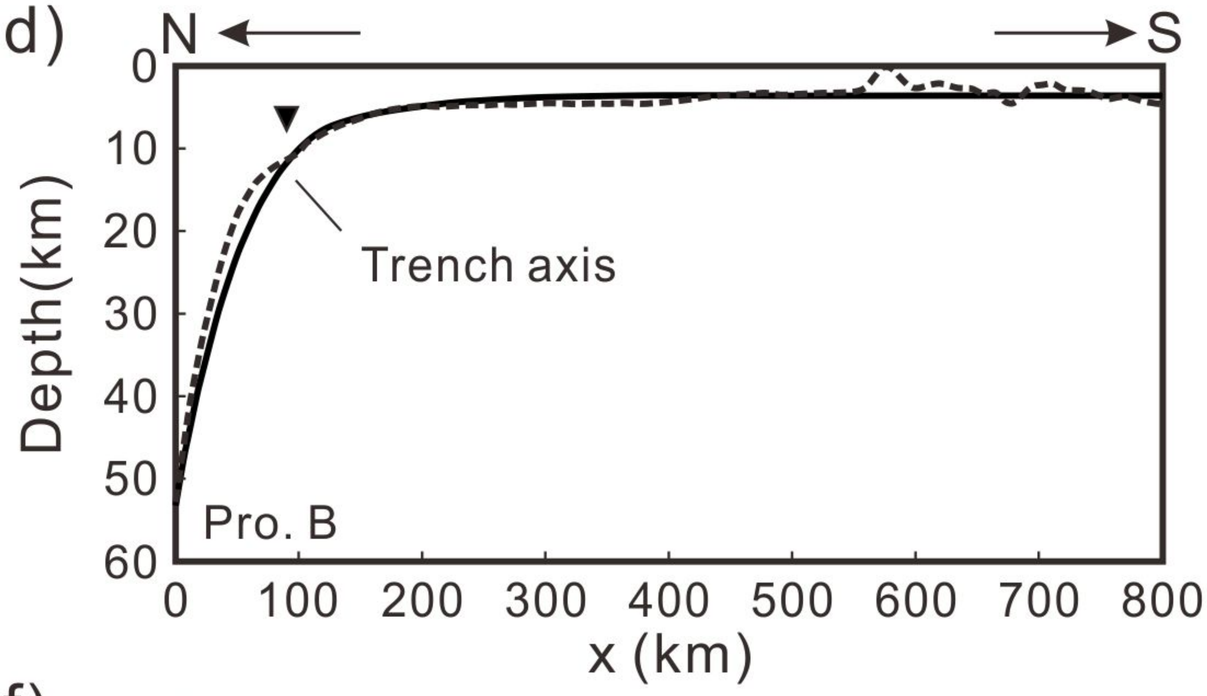
N
S
Depth(km)
0
10
20
30
40
50
60
Trench axis
Pro. B
0
100
200
300
400
500
600
700
800
x (km)

e)

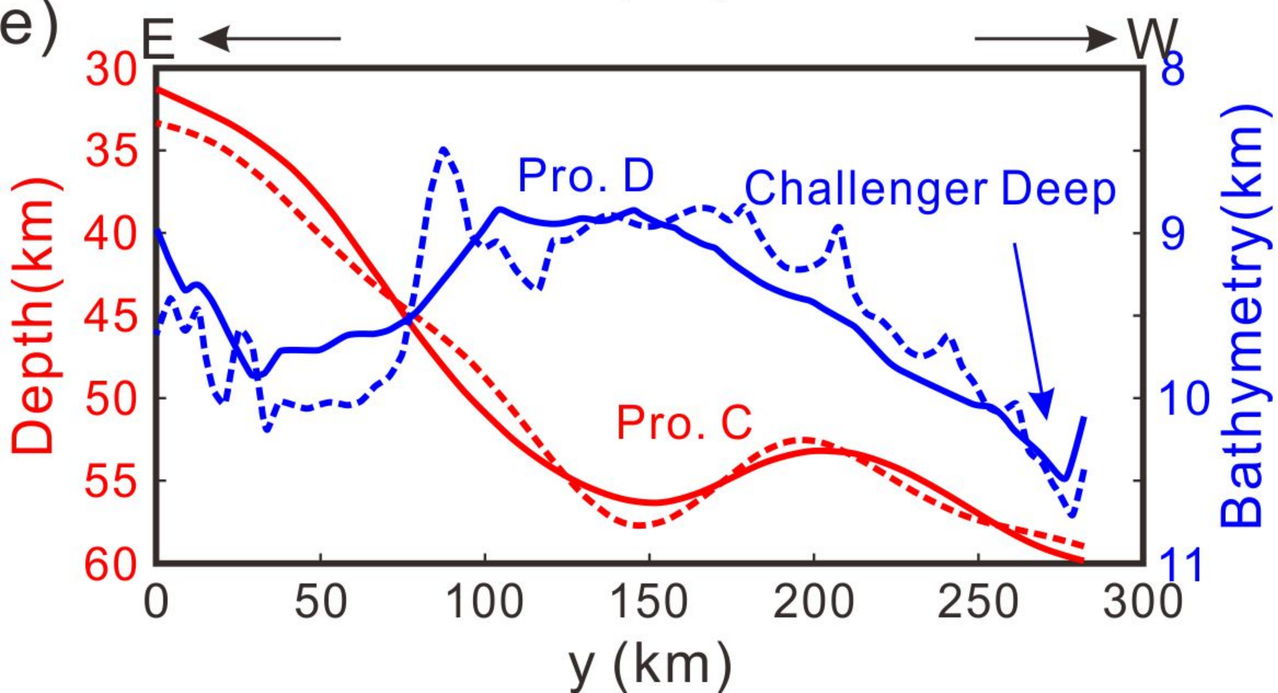
E
W
Depth(km)
30
35
40
45
50
55
60
Pro. D
Challenger Deep
Pro. C
Bathymetry(km)
8
9
10
11
0
50
100
150
200
250
300
y (km)

f)

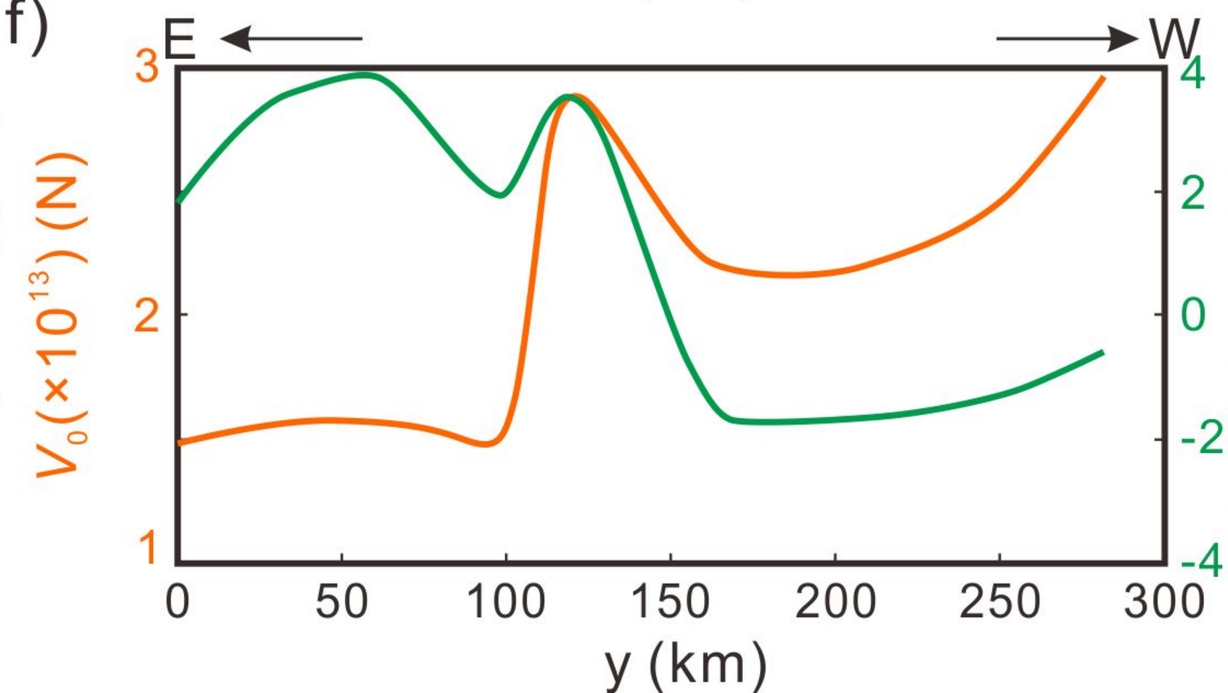
E
W
V_0(×10^{13}) (N)
3
2
1
M_0(×10^{17}) (Nm)
4
2
0
-2
-4
0
50
100
150
200
250
300
y (km)

Figure03.

(a)

(b)

(c)

(d)

(e)

from Zhu et. al (2019)

from USGS

from GCMT

Mariana trench

Challenger Deep

σ^{e}_{xx}

σ^{e}_{yy}

σ^{e}_{xy}

σ^{e}_{1}

×10³ MPa

12°00'

11°30'

11°00'

10°30'

142°30'

143°00'

143°30'

144°00'

A

A'

W

E

Stress(×10³ MPa)

Depth (km)

Distance (km)

Seismic counts

Depth(km)

Figure04.

(a)

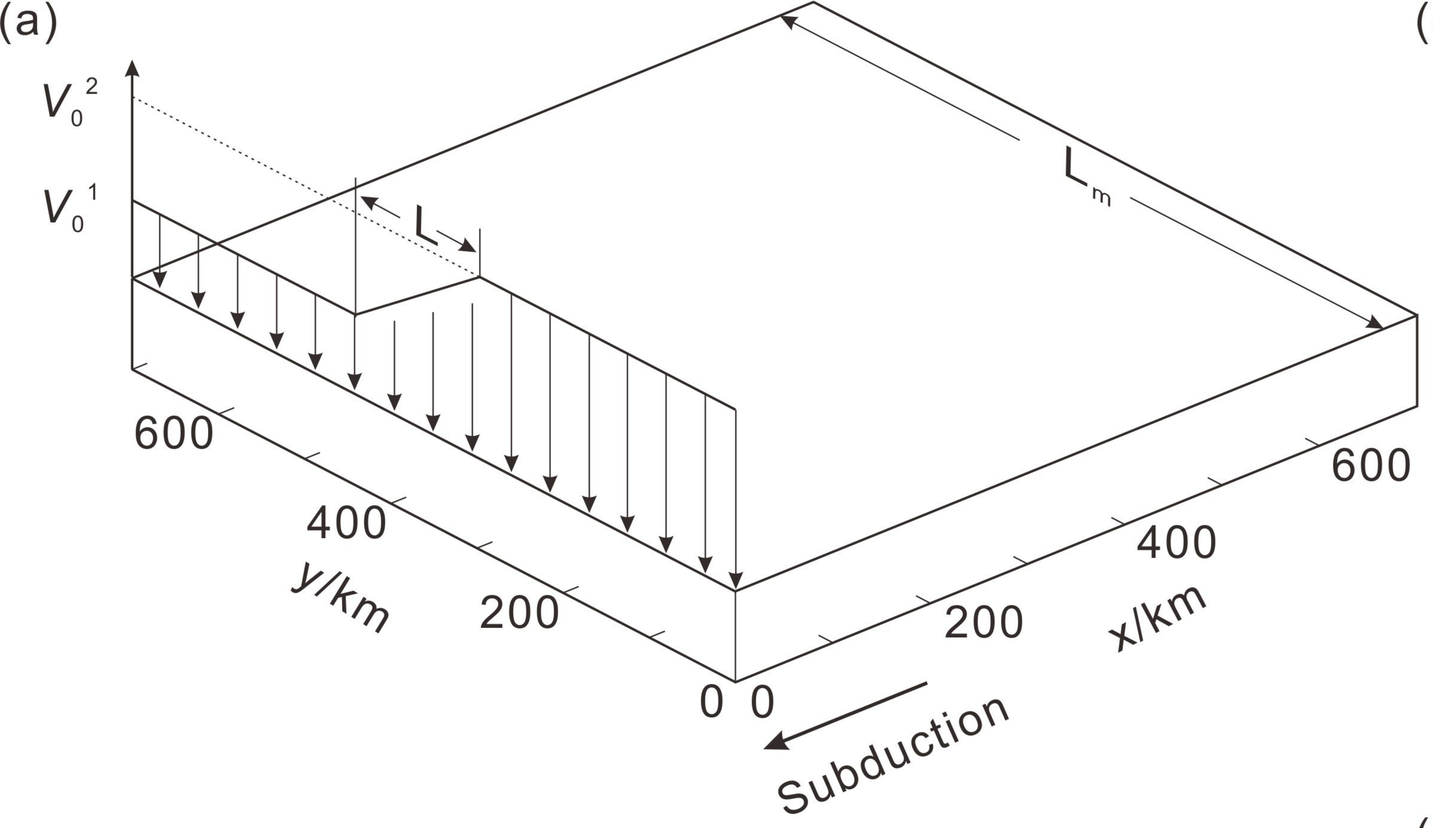
V_0^2
V_0^1
L
L_m
600
400
y/km
200
0
0
200
400
x/km
600
Subduction

(b)

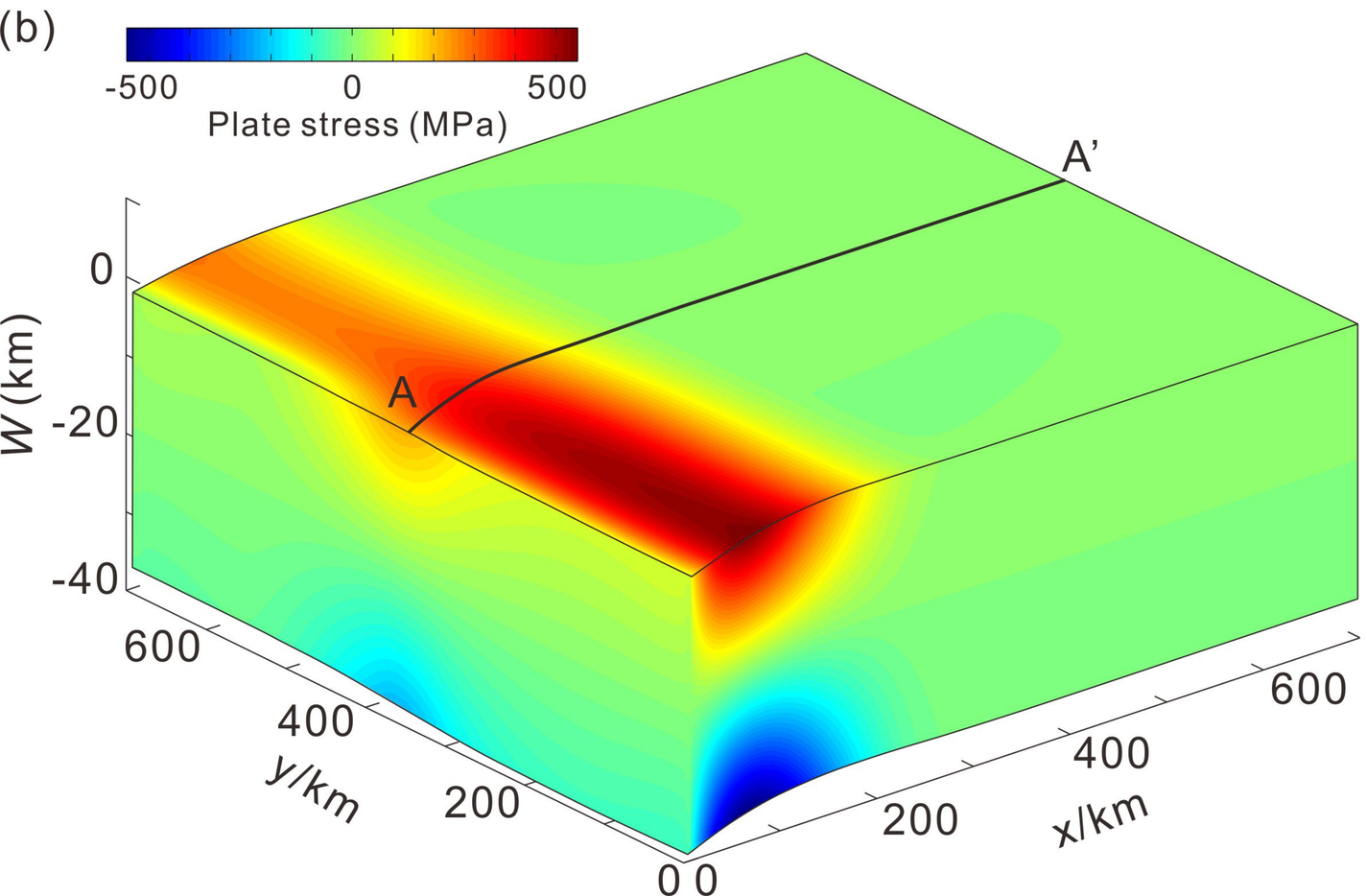
-500
0
500
Plate stress (MPa)
A'
A
0
-20
-40
W (km)
600
400
y/km
200
0
0
200
400
x/km
600

(c)

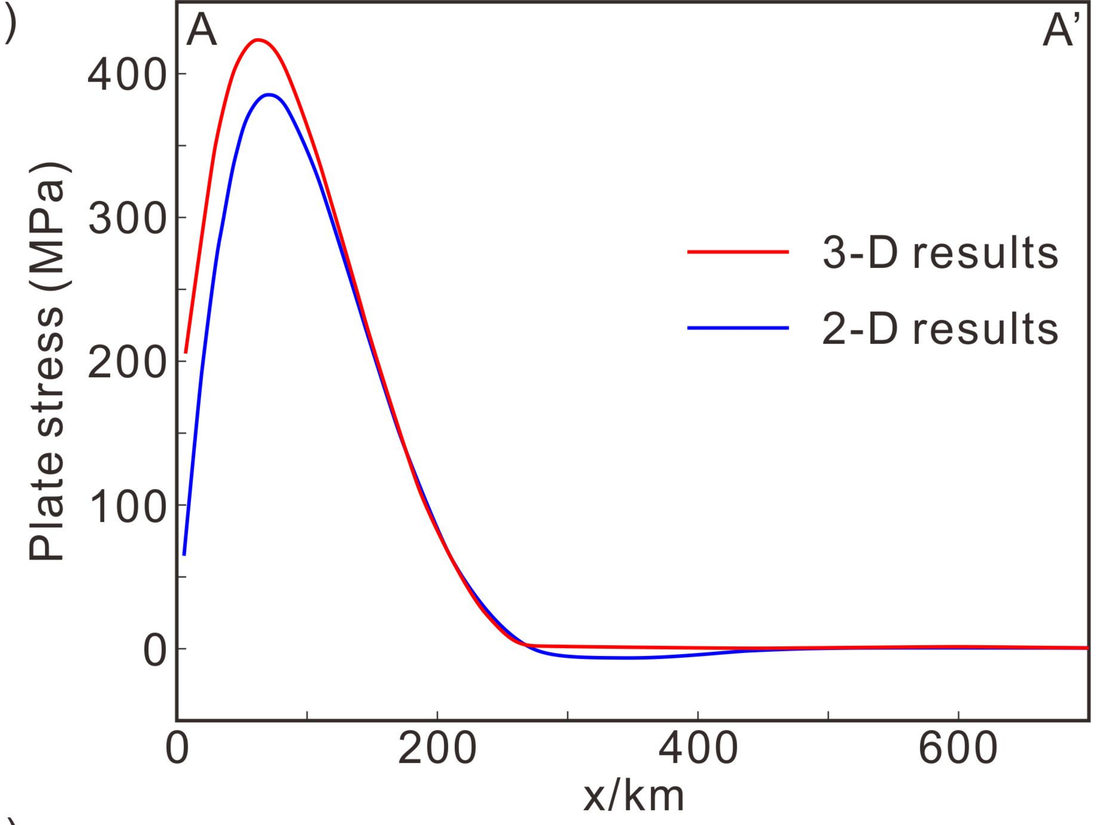
A
A'
400
300
200
100
0
Plate stress (MPa)
3-D results
2-D results
0
200
400
600
x/km

(d)

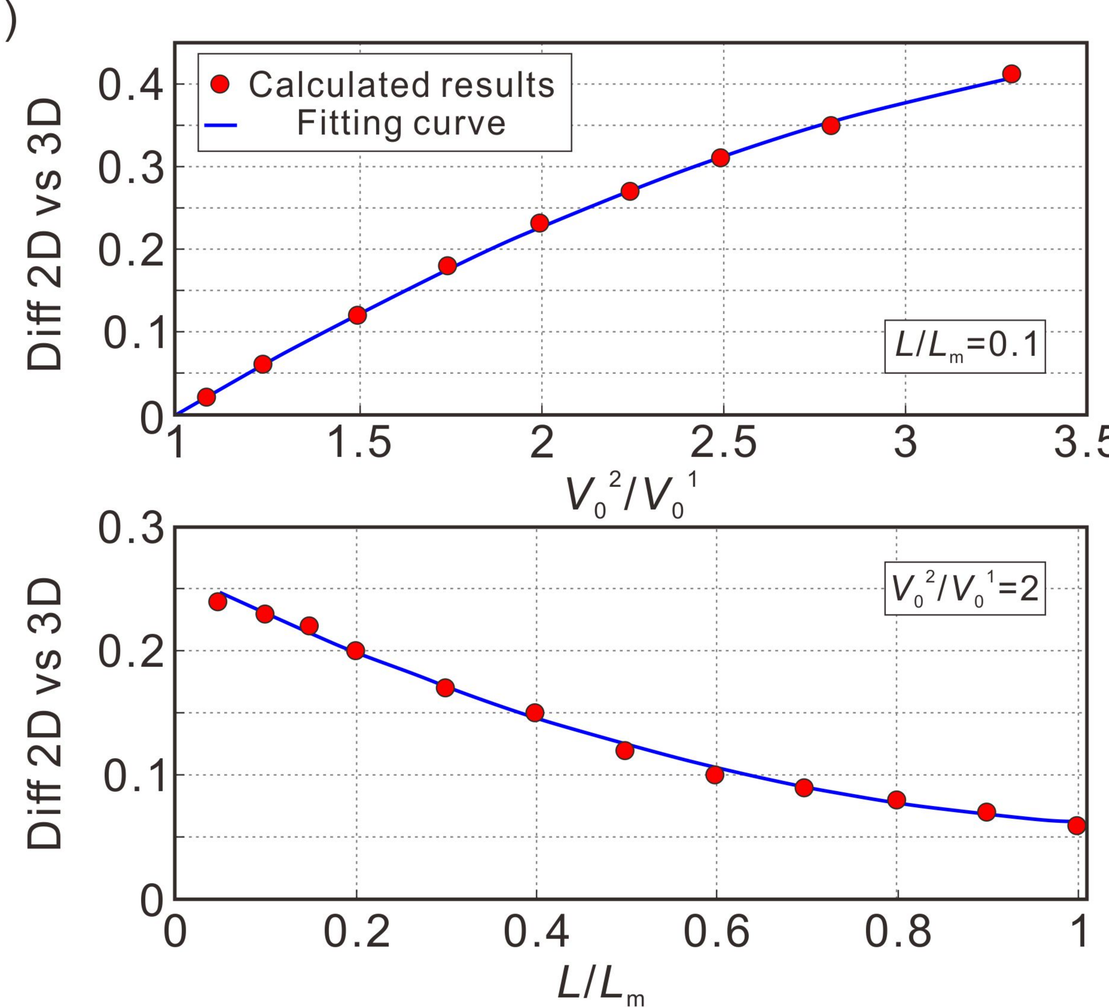
Calculated results
Fitting curve
L/L_m=0.1
Diff 2D vs 3D
0.4
0.3
0.2
0.1
0
1
1.5
2
2.5
3
3.5
V_0^2/V_0^1
V_0^2/V_0^1=2
Diff 2D vs 3D
0.3
0.2
0.1
0
0
0.2
0.4
0.6
0.8
1
L/L_m

Figure05.

(a)

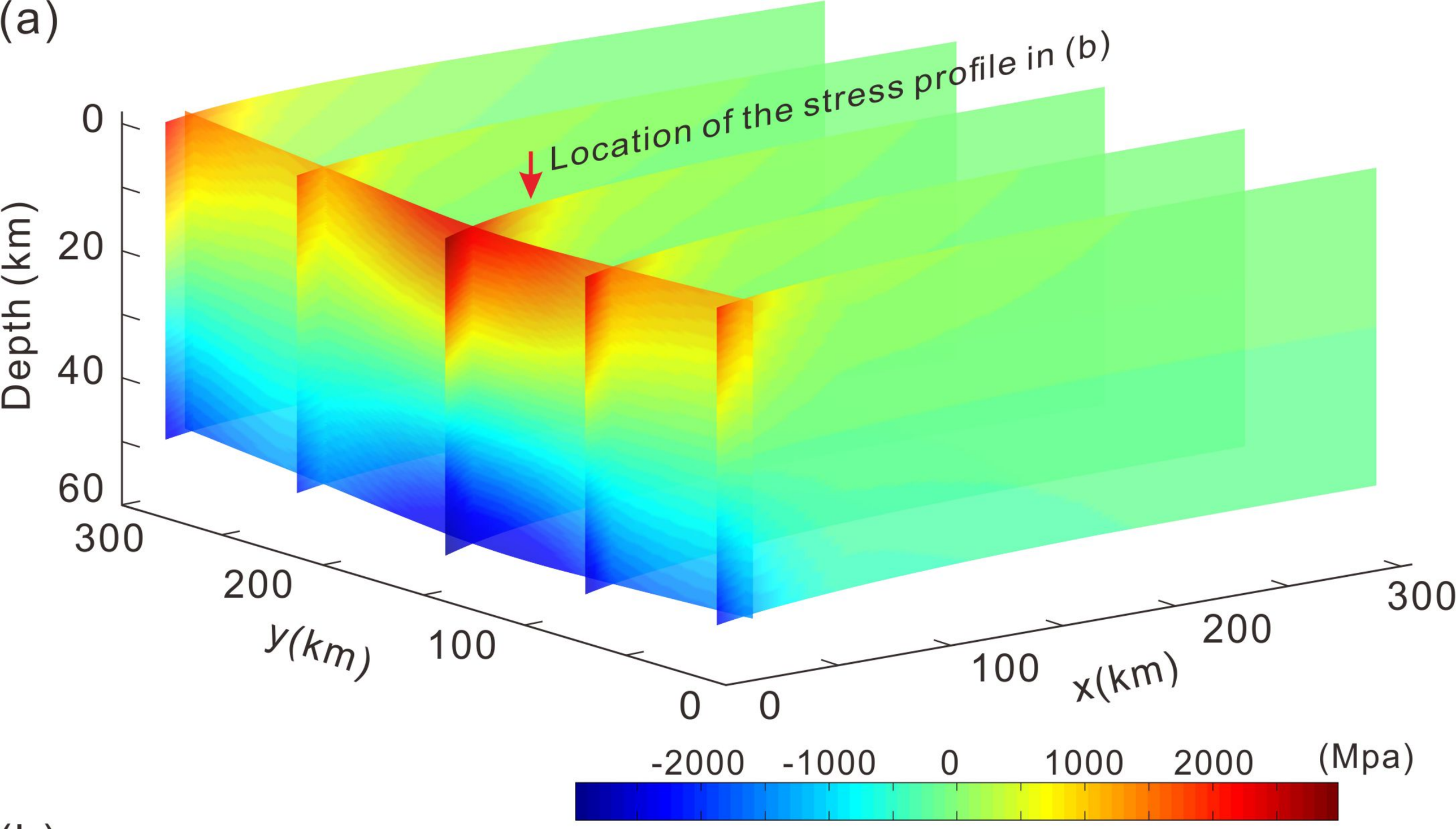
Location of the stress profile in (b)
Depth (km)
0
20
40
60
300
200
y(km)
100
0
0
100
200
300
x(km)
-2000
-1000
0
1000
2000
(Mpa)

(b)

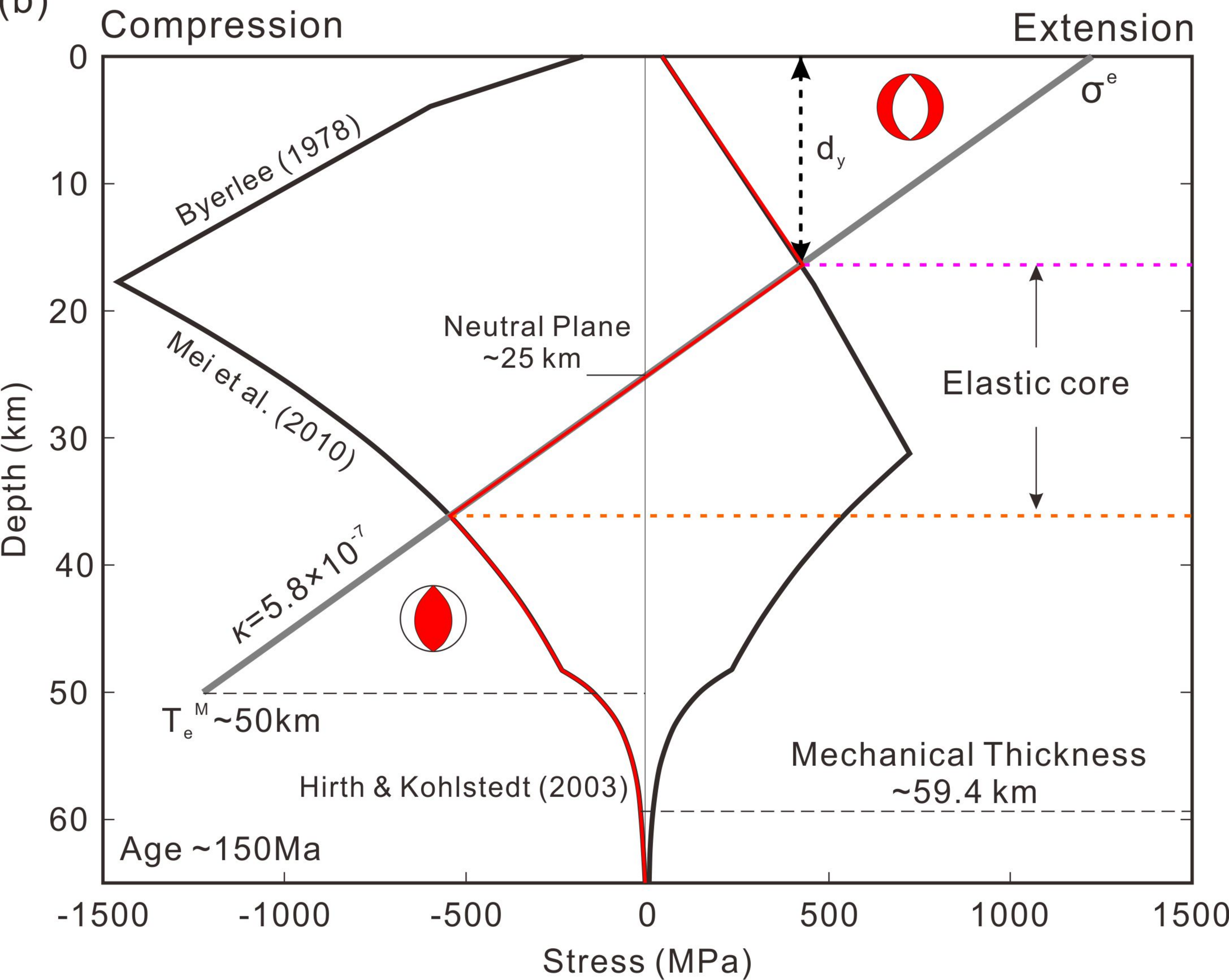
Compression
Extension
Byerlee (1978)
Mei et al. (2010)
Neutral Plane
~25 km
d_y
σ^e
Elastic core
κ=5.8x10^{-7}
T_e^M~50km
Hirth & Kohlstedt (2003)
Mechanical Thickness
~59.4 km
Age ~150Ma
Depth (km)
0
10
20
30
40
50
60
-1500
-1000
-500
0
500
1000
1500
Stress (MPa)